JOURNAL OF MATERIALS SCIENCE 33 (1998) 755–762

LaB_6 and TiB_2 electrodes for the alkali metal thermoelectric converter

K. TSUCHIDA, T. NAGATA, H. NAKATA, A. KATO
Department of Chemical Science and Technology, Faculty of Engineering, Kyushu University, Fukuoka 812-81, Japan

LaB_6 and TiB_2 electrodes for the alkali metal thermoelectric converter (AMTEC) were prepared from the respective powders by a screen-printing method and their electrode properties were investigated. Optimum values were obtained for particle size, thickness and porosity of electrode. When the vacuum level of the low-temperature side of the AMTEC increased above 10 Pa, the power density decreased remarkably. These results can be interpreted as different electrode processes in the AMTEC: (1) a charge transfer process, (2) surface diffusion on the electrode, (3) desorption from electrode particles, and (4) vapour-phase diffusion in the electrode pore. The maximum power density was 0.54 W cm^{-2} (LaB_6) and 0.24 W cm^{-2} (TiB_2) at 800 °C. © *1998 Chapman & Hall*

1. Introduction

The alkali metal thermoelectric converter (AMTEC) is a device for direct conversion of thermal to electric energy and gives high power density and high efficiency [1–7]. AMTEC contains sodium as the working fluid and is divided into a high-temperature region (900–1300 K) and a low-temperature region (400–800 K) by a β″-alumina solid electrolyte (BASE) separator. A schematic diagram of AMTEC is shown in Fig. 1. In the high-temperature region, liquid sodium contacts directly with BASE and works as an anode. Sodium ionizes at the interface between liquid sodium and BASE and Na^+ ions are transmitted through the BASE. On the opposite side of the BASE, Na^+ ions recombine with electrons on the porous electrode, and sodium vaporizes into the vacuum. Sodium gas condenses on a condenser in the low-temperature region and liquid sodium is circulated by a pump to the high-temperature region. AMTECs driving force is the difference in sodium activities between high and low-temperature regions. In the high-temperature region, the resistance between liquid sodium and BASE is considered to be very small. Therefore, the performance of the AMTEC is essentially affected by that of cathode. The electrode for the AMTEC must have a low electrical resistance, suitable porosity, and high stability. Although molybdenum porous electrode, made by sputtering, gives high power density, molybdenum changes into several kinds of Na–Mo–O compounds during AMTEC operation and evaporates, resulting in a decrease of AMTEC lifetime [8,9].

We had investigated the interaction of nitrides and carbides of several transition metals (IV, V and VI groups) with β″-alumina (900 °C) or liquid sodium (700 °C) with the objective of finding better electrodes for AMTEC. The result showed that TiN, TiC, NbN and NbC were stable at the AMTEC operating temperature and are potential candidates for long-life AMTEC electrode materials [10]. We also prepared porous films by a printing method from powders of these materials and examined their characteristics in AMTEC cells [11–15]. These works showed that ceramic electrodes work well. We calculated the exchange current density, I_0, using Equation 1 for several AMTEC electrodes

$$I_0 = IRT/\eta F \quad (1)$$

where I is the current density, R the gas constant, T the temperature, η the cathodic overvoltage, and F the Faraday constant. Activation energies of each electrode were calculated from an Arrhenius plot of exchange current densities. We showed that the activation energies were lower for a ceramic electrode than for the molybdenum electrode and that there is a linear relation between the activation energy and work function of electrode materials [16]. Therefore, we selected LaB_6 which has a low work function, and examined the electrode characteristics. Furthermore, the TiB_2 electrode which had been used for AMTEC by Fang and Knodler [17] was also investigated for comparison.

2. Experimental procedure

2.1. Preparation of the electrode

To examine the stability of LaB_6 and TiB_2 for β″-alumina and liquid sodium, pellets of a mixture of LaB_6 or TiB_2 and β″-alumina powders were heated at 900 °C for 5 h in an Ar–H_2 atmosphere or heated at 700 °C for 8 h in liquid sodium under an argon atmosphere. X-ray diffraction (XRD) on pellets after heating showed that no new phase was detected in either the LaB_6 or TiB_2 samples, indicating their

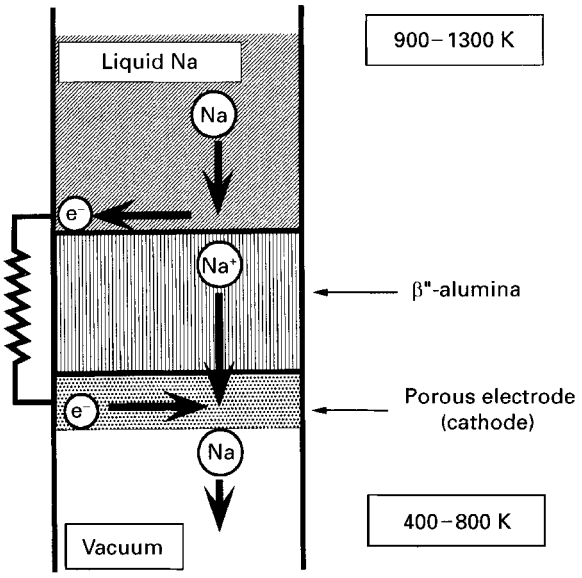

Figure 1 Schematic diagram of AMTEC.

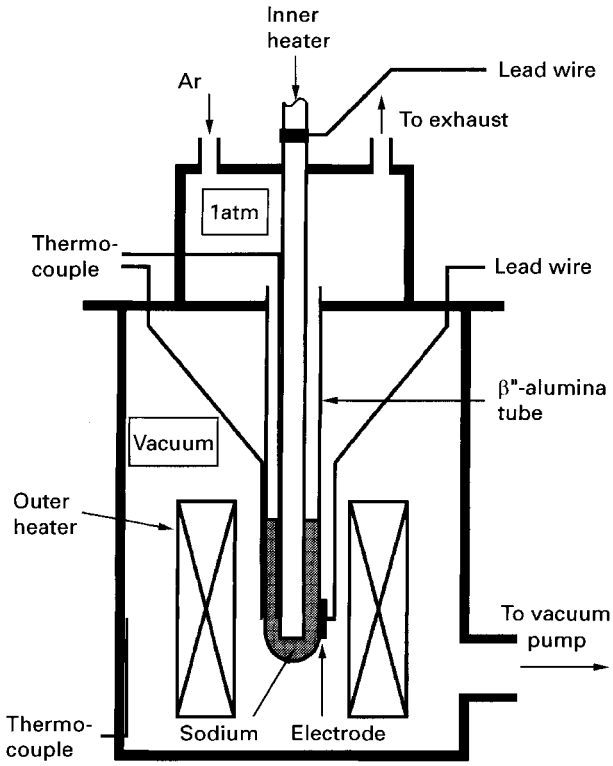

Figure 2 The AMTEC apparatus used in this work.

stability for β″-alumina and liquid sodium under AMTEC operating conditions.

Three kinds of LaB_6 powders (particle size: A, 4.5 μm; B, 0.6 μm; C, 0.2 μm) obtained by sedimentation in ethyl alcohol from commercial LaB_6 powder (Japan New Metals Co. Ltd). Commercial TiB_2 powder (Japan New Metals Co. Ltd, particle size 1–2 μm) was used. These powders were mixed with an organic vehicle (terpineol + ethylcellulose (10 wt %)) and the resulting paste was printed on to BASE tube (Ceramatec Inc., o.d. 15 mm, thickness 1 mm and length 200 mm) through a screen mesh (RISO Kagaku Co., Hi-mesh master, 200 mesh), or applied directly with a brush. The paste film was levelled for 10 min and dried at 150 °C in air for 15 min. The film was fired in $Ar–H_2$ (80:20 ml min^{-1}) for 1 h at 900 °C. LaB_6 and TiB_2 films prepared on α-alumina (KYOCERA, A-476) using similar conditions, were analysed by XRD and observed by scanning electron microscopy (SEM).

2.2. AMTEC operation and electrochemical measurement

The apparatus used in the present work is shown in Fig. 2. The chamber was made of stainless steel. The high-temperature chamber was filled with argon gas (1 atm) and the low-temperature chamber was evacuated with a rotary pump and an oil diffusion pump. This pumping system maintained its pressure at 10^{-3}–10^{-1} Pa during AMTEC operation. Molybdenum mesh (30 mesh) was placed on the electrode and molybdenum lead wires (for voltage and current) and tied with molybdenum wire. The Chromel–Alumel (CA) thermocouple was also tied. The BASE tube with the electrode was set into the AMTEC apparatus. After a preliminary heat treatment (in vacuum, 450 °C), 6–8 g sodium was introduced in the BASE tube and heated by two heaters (inner and outer).

The temperature of liquid sodium in the BASE tube, electrode surface and the wall of the apparatus were monitored by the CA thermocouple. The voltage–current profiles were measured by cyclicvoltammetry (sweep rate 5 mV s^{-1}) with potentiostat/galvanostat (Hokuto Denko Ltd, HA-501G) and arbitrary function generator (Hokuto Denko Ltd, HB-105). A.c. impedence measurements of the AMTEC cell were carried out with a frequency response analyser (Solartron, FRA1250) and potentiostat (HA-501G) in the frequency range 65 kHz to 0.1 Hz or 0.01 Hz. A microcomputer (Epson, PC-286VG) controlled all measurement devices with a GPIB(IEEE488) interface. The pressure of the lower temperature chamber was controlled by introduction of argon gas by a mass flow control valve, if necessary.

3. Results and discussion

3.1. Effect of particle size

To examine the effect of particle size, three kinds of paste were prepared by using three kinds of LaB_6 powder (powder content 20 wt %). LaB_6 films prepared on α-alumina substrate (Kyocera, A-476) from each powder are shown in Fig. 3. The average thickness of these electrodes was 7 μm (LaB_6–A), 5 μm (LaB_6–B) and 6 μm (LaB_6–C).

The electrode characteristics were examined during AMTEC operation. Fig. 4 shows current–voltage profiles of three electrodes. Fig. 5 shows the relation between current and overvoltage. Overvoltage was calculated by subtracting IR drop from the total voltage drop. The LaB_6–B electrode showed the highest power density of the three electrodes. The

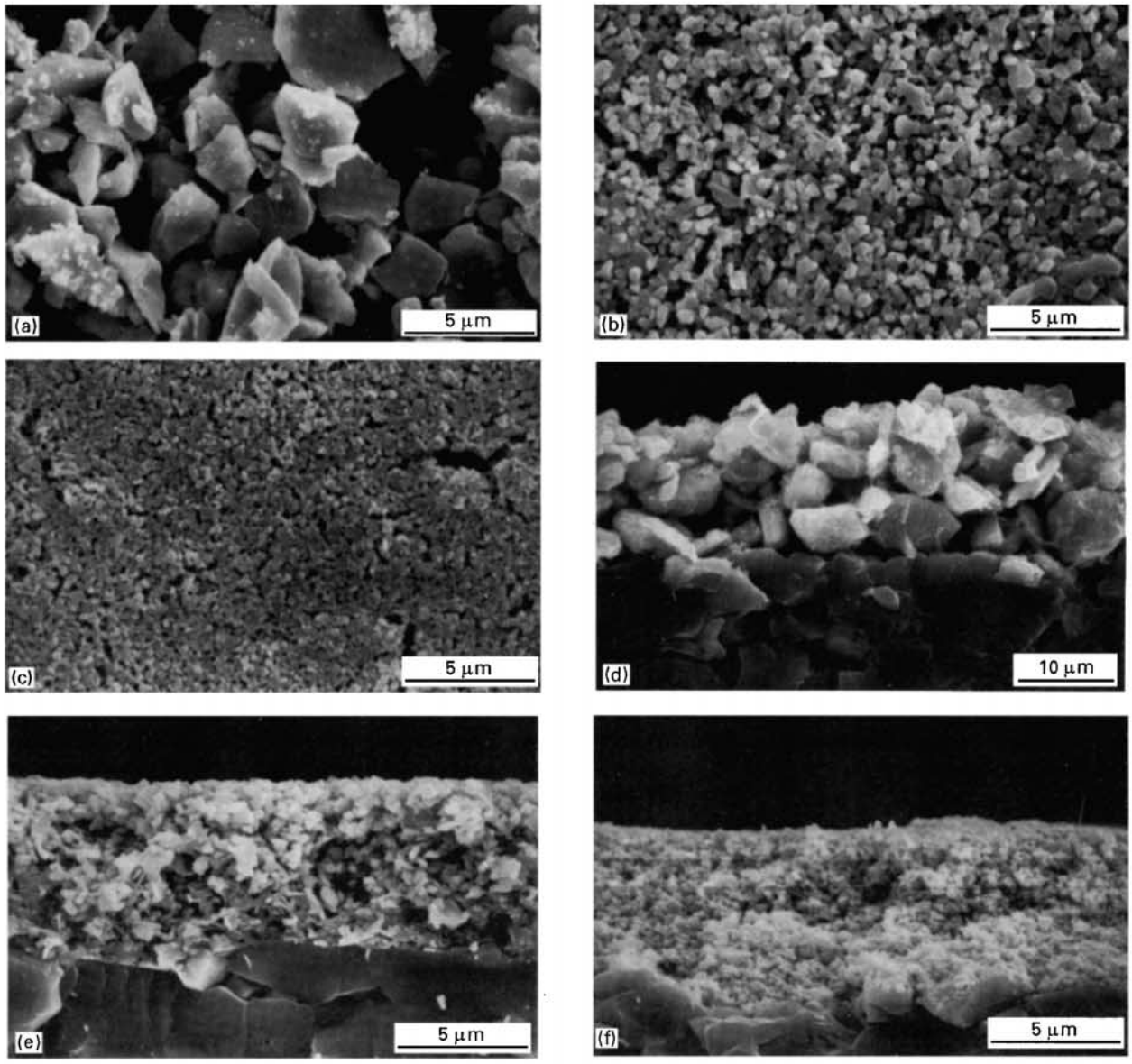

Figure 3 Scanning electron micrographs of LaB_6 film on α-alumina substrate (fired at 900 °C for 1 h in an $Ar–H_2$ atmosphere): (a,d) LaB_6–A, (b,e) LaB_6–B, and (c,f) LaB_6–C.

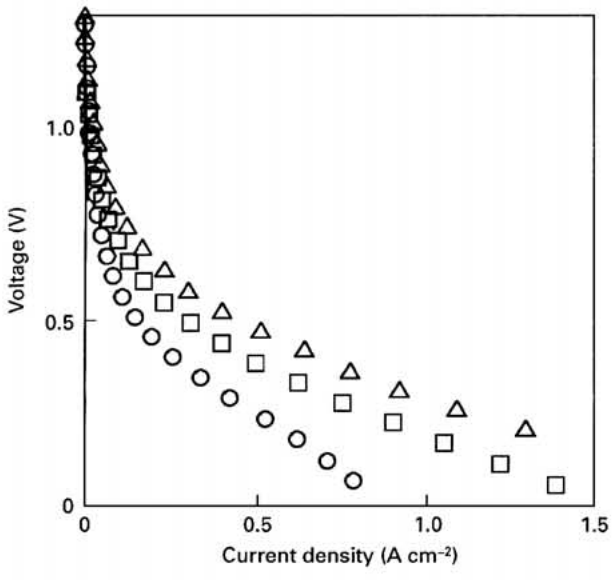

Figure 4 The effect of electrode grain size on the voltage–current profiles (750 °C). (○) 0.2 μm, (△) 0.6 μm, (□) 4.5 μm.

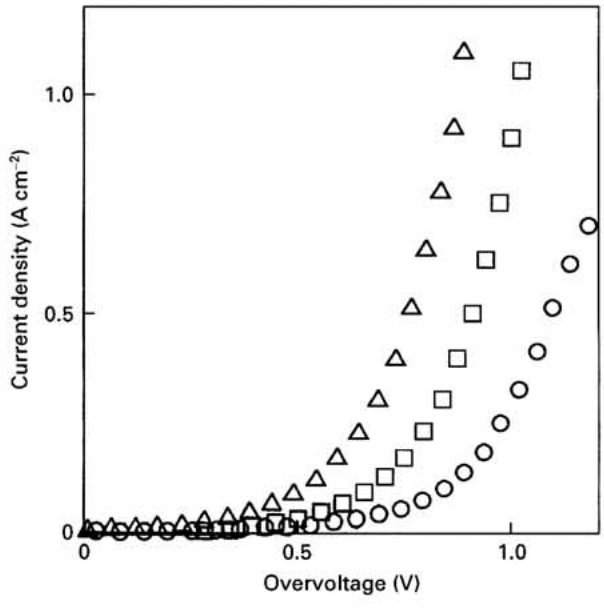

Figure 5 The effect of electrode grain size on the relation between current and overvoltage (750 °C). (○) 0.2 μm, (△) 0.6 μm, (□) 4.5 μm.

maximum power density with the LaB_6–B electrode was 0.54 W cm^{-2} (800 °C) and 0.28 W cm^{-2} (750 °C).

3.2. Effect of electrode thickness

Mass transportation in the electrode is related to AMTEC properties. The thickness of the electrode affects sodium diffusion in the electrode. Three LaB_6 electrodes which have different thicknesses (2, 5 and 12 μm) were prepared from LaB_6–B powder. Fig. 6 shows the effect of thickness of electrode on the relation between voltage and current density of AMTEC with LaB_6–B electrodes. This result agreed with the case of a TiC electrode [18]. Fig. 7 shows the relation between maximum power density of AMTEC at 750 °C and electrode thickness. The results for the TiC electrode [18] are also shown in Fig. 7. Both the TiC and LaB_6–B electrodes showed a maximum power density at a thickness of about 5 μm. Fig. 8 shows a Cole–Cole plot of a.c. measurement at an electrode thickness of 12 μm. R_t is the ohmic resistance of the cell and R_{ct} is the resistance due to electrode processes which include charge transfer and mass transportation processes. The results of a.c. impedance measurements are summarized in Table I. R_t was nearly equal to the calculated resistance of β″-alumina (0.169 Ω cm^2) at the electrodes which were 5 and 12 μm thick. On the 2 μm thick electrode, R_t seems to be increased because of increase in the contact resistance of the electrode to BASE. When the electrode thickness was 12 μm, R_{ct} increased due to the effect of pressure drop for the sodium flow in the electrode pores.

3.3. Effect of porosity of the electrode

Three electrodes having different porosities were prepared and the effect of porosity on AMTEC performance was investigated. By using LaB_6–B powder, three kind of pastes with powder contents of 10, 20 and 30 wt % were printed on BASE and fired as above, resulting in three electrodes having different porosity. Fig. 9 shows scanning electron micrographs of these films on α-alumina substrate. The porosity of the electrode was calculated from the amount of LaB_6 printed on the substrate, the thickness of the film (SEM observation) and the theoretical density of LaB_6(4.72 g cm^{-3}) [19]. The porosities of the three electrodes were 64% (10 wt %), 55% (20 wt %) and

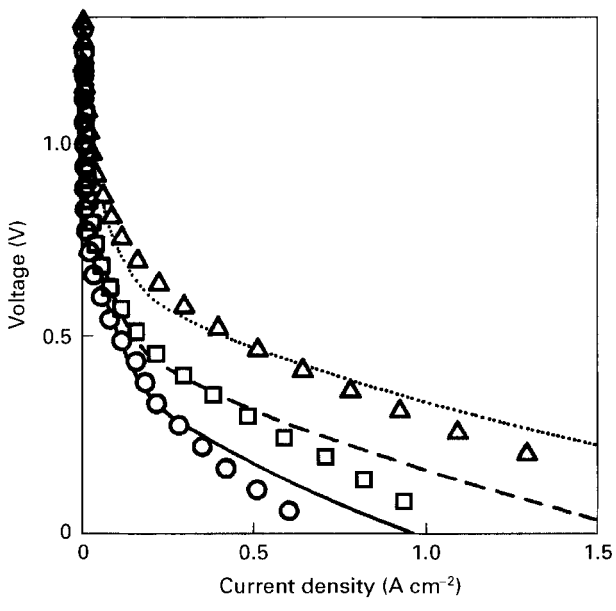

Figure 6 The effect of electrode thickness (LaB_6–B) on the voltage–current profile and calculated profiles from Equation 4 (750 °C). (—○—) (– –△– –) 5 μm, (— □ —) 12 μm.

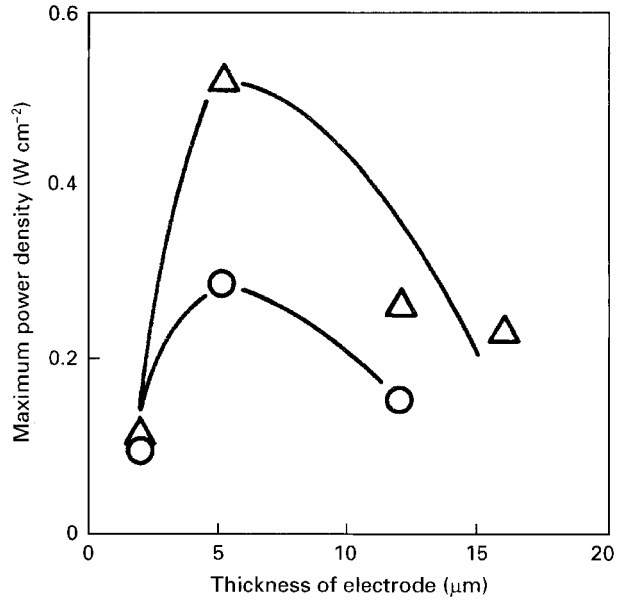

Figure 7 The relation between maximum power density of AMTEC and electrode thickness (750 °C). (○) LaB_6–B, (△) TiC.

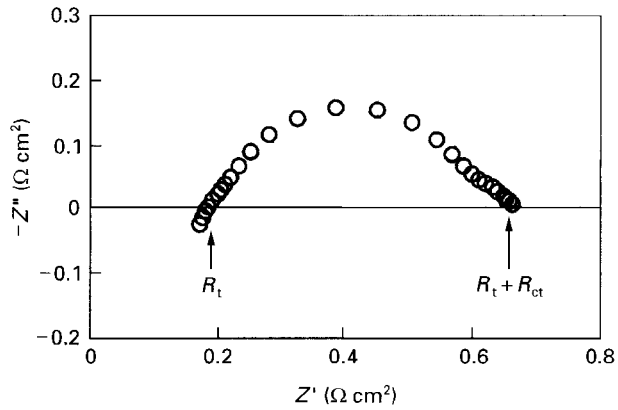

Figure 8 A Cole–Cole plot of AMTEC with an LaB_6–B electrode (thickness 12 μm) at 750 °C.

TABLE I Relation between the thickness of the electrode and resistance (750 °C)

Thickness (μm)	R_t (Ω cm^2)	R_{ct} (Ω cm^2)
2	0.25	0.63
5	0.15	0.20
12	0.18	0.49
β″-alumina	0.169	–

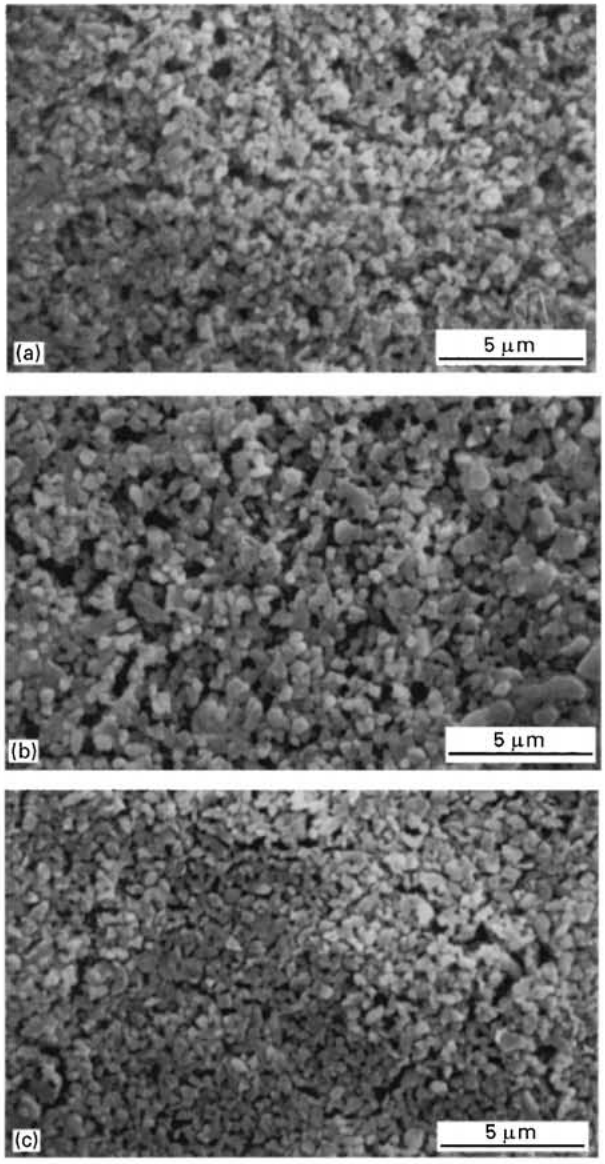

Figure 9 Scanning electron micrographs of LaB_6–B film having various porosities on α-alumina substrate (fired at 900 °C for 5 h in an Ar–H_2 atmosphere): (a) powder content in paste 10 wt %, porosity 64%; (b) powder content in paste 20 wt %, porosity 55%; (c) powder content in paste 30 wt %, porosity 21%.

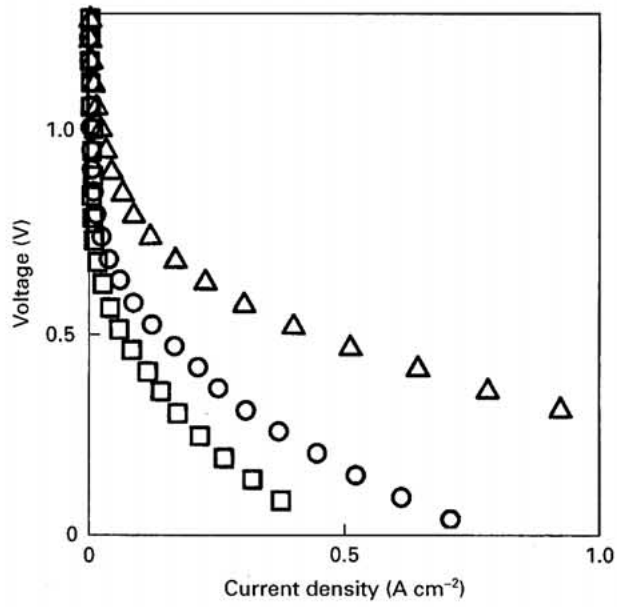

Figure 10 The effect of porosity on the voltage–current profiles of AMTEC with LaB_6–B electrode (750 °C). Powder content/porosity: (○) 10 wt % / 64%; (△) 20 wt % / 55%; (□) 30 wt % / 21%.

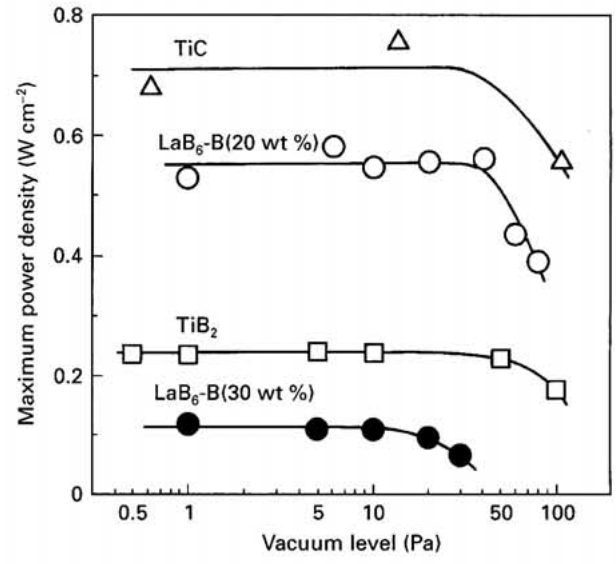

Figure 11 The effect of vacuum level on the maximum power density of AMTEC (800 °C).

21% (30 wt %). Fig. 10 shows voltage–current profiles of each electrode. The electrode with 55% porosity showed the best performance of the three.

3.4. Effect of vacuum level of the low-temperature chamber

The vacuum level of the low-temperature chamber influences sodium transport. Relations between maximum power density and vacuum level on LaB_6 and TiB_2 electrodes are shown in Fig. 11. The result for the TiC electrode [18] is shown for comparison. Each electrode showed the same tendency with the vacuum level, which had little effect on the power density below 10 Pa, but above 10 Pa, the power density decreases as the vacuum level becomes poor. Assuming a representative length of the flow (L_M) as twice the electrode thickness, the Knudsen number (λ/L_M, λ is the mean free path) is calculated as 100–300 at 10 Pa and at 750 °C. Consequently, the flow of sodium vapour is by free molecular flow below 10 Pa, but may be affected by viscous flow above 10 Pa.

3.5. Cathode process

In the present work, the effects of grain size, thickness and porosity of the electrode, and the vacuum level of the low-temperature chamber on AMTEC properties, were found to be important. The cathode process in the AMTEC may consist of the following four processes:

1. charge transfer ($Na^+ + e^- \rightarrow Na(ad)$ at the BASE/electrode interface;

2. surface diffusion of Na(ad) on the grain-consisting electrode;

3. desorption of Na(ad) from the grain surface;

4. vapour-phase diffusion of Na(g) in the electrode pores toward the low-temperature chamber.

In order to obtain a high power density, each of the four consecutive processes must proceed at a high rate. The effect of vacuum level of the low-temperature chamber on the power of the AMTEC becomes appreciable in the region of viscous flow above 10 Pa, as seen in Fig. 11. On the other hand, the vacuum level does not affect the power below 10 Pa where the flow of sodium vapour in the porous electrode is considered to be free molecular flow. The effect of electrode structures (grain size, thickness and porosity) on the power of the AMTEC observed under 10^{-3}–10^{-1} Pa, may be interpreted as follows.

The presence of an optimum value for the particle size of electrode materials may be explained by a charge transfer process. The charge transfer process in the AMTEC cathode occurs at the triple-phase boundary of BASE/porous electrode/sodium gas phase. Consequently, the overvoltage decreases with increase in the length of the triple-phase boundary. The electrode with a finer grain size will have a longer triple-phase boundary. However, when the particle size is finer than the optimum one, the pore size in the electrode becomes smaller and cause a large resistance for sodium vapour transportation.

There is an optimum value for porosity of an electrode. This may also be explained by the changes in the resistance for sodium vapour transportation in the electrode pores and the length of the triple-phase boundary for charge transfer, as above. At a dense electrode (21% porosity), the diffusion resistance of sodium vapour becomes large and governs the power of AMTEC. On the other hand, at the electrode with 64% porosity, the reduced length of the triple-phase boundary may limit the charge-transfer rate.

There was an optimum electrode thickness, as shown in Fig. 7. When sodium diffusion in the electrode pores is free molecular flow and the electrode pores are cylindrical, the pressure drop, ΔP, across the electrode film is expressed as [7]

$$\Delta P = 0.75G(MRT_h/2\pi)^{1/2} I/F \quad (2)$$

$$G = 8l/(d^3N) \quad (3)$$

where M, is the molecular weight of sodium, R the gas constant, I the current density, F the Faraday constant, and T_h the temperature of the high-temperature side. G is a dimensionless parameter for the electrode structure, defined by the diameter of a pore, d, the length of a pore, l, and the number of pores per unit area, N. By means of these equations, the pressure drop, ΔP, was calculated at 750 °C, and voltage–current profiles were calculated using the Nernst equation (Equation 4).

$$V = \frac{RT_h}{F} \ln \frac{P_h}{(T_h/T_l)^{1/2} P_l + (2\pi MRT_h)^{1/2}(I/F) + \Delta P} - R_0 I \quad (4)$$

T_l is the temperature of the low-temperature side, P_h and P_l are vapour pressures of sodium at temperatures T_h and T_l, and R_0 is the internal resistance of the cell. The calculated voltage–current profiles were fitted by changing G. The results are shown in Fig. 6, where the values of R_i given in Table I were used in place of R_0. The values of G were calculated as 4000 (electrode thickness 2 μm), 250 (5 μm) and 1300 (12 μm). By assuming that l is the thickness of the electrode, $d = 0.5$ μm and $N = 0.7$ μm^{-2}, G is found to be 183 (2 μm), 457 (5 μm) and 1097 (12 μm). Williams *et al.* [20] and Tanaka *et al.* [7] had reported that the value of G from curve fitting is smaller than that from observation of the electrode. They considered that it may be due to the ionic conductivity of Na_2MoO_4. In the present work, there was no ionic conductivity in the LaB_6 electrode because LaB_6 reacts little with sodium, and G values from curve fitting for the 5 or 12 μm thick electrodes are nearly equal to that from SEM observation. On the other hand, G from curve fitting for the 2 μm thick electrode is nearly 20 times larger than that from SEM observation. It is suggested that mass transfer of sodium in the porous electrode, which consists of small grains, is not only due to a vapour–phase diffusion in the electrode pore, but there is also a contribution of diffusion on the surface of the electrode grains. The covering rate, Θ, of electrode by sodium was calculated by Williams *et al.* [21] as follows

$$\Theta = \exp\{-[(kT/hD_s)\exp(-E_D RT)]^{1/2} z\} \quad (5)$$

where D_s is the surface diffusion coefficient of sodium, k is Boltzmann's constant, T is the temperature, h is Planck's constant, E_D is the activation energy for desorption and z is the distance from the BASE–electrode interface. The calculation showed that the surface diffusion consist for the most part of mass transportation of sodium at 750 °C, especially for an electrode thickness of less than 2–3 μm. For an electrode thickness of under 2–3 μm, the number of sites of sodium desorption decreases with decreasing number of grains in the electrode. Thus, when the thickness of the electrode was 5 μm, overvoltage was the smallest, at a given current density, of the three electrodes having different thicknesses. The negative deviation of the observed voltage–current curve from that calculated at high current density in Fig. 6, may be limiting current from mass transport. The rate-determining step in the cathode processes may be the desorption from the electrode grain (electrode thickness 2 μm) or vapour–phase diffusion in electrode pores (5 and 12 μm).

3.6. TiB_2 electrode

TiB_2 electrode was prepared by using TiB_2 Powder (1.7 μm). The powder content of TiB_2 in the paste was 20 wt %, and the electrode thickness was 5 μm. Fig. 12 shows scanning electron micrographs of TiB_2 film on α-alumina substrate prepared by the same procedures as the electrode. The structure of this film is similar to the LaB_6–A electrode. Fig. 13 shows voltage–current profiles of the TiB_2 electrode. The maximum power

density with the TiB_2 electrode was 0.24 W cm^{-2} (800 °C) and 0.17 W cm^{-2} (750 °C). From an Arrhenius plot of the exchange current density, calculated using Equation 1, the activation energy for TiB_2 electrode was calculated. Table II shows the activation energies in the present work (LaB_6, TiB_2 and Mo [18]). These values were also much lower for the TiC electrode [15,16,18] than those of metal electrodes, indicating that ceramic materials are potential electrodes for AMTEC.

4. Conclusions

1. LaB_6 and TiB_2 have a low reactivity for β″-alumina and sodium. These materials have lower activation energy than that of metal, indicating that LaB_6 and TiB_2 are potential candidates for AMTEC electrodes.

2. Optimum values exist for electrode grain size, thickness and porosity for an electrode. When the vacuum level of the low-temperature chamber is below 10 Pa, the power density decreased with decreasing vacuum level, because the flow of sodium in the vapour phase becomes viscous flow. These results can be interpreted from the resistance in the electrode processes: charge transfer at a triple-phase boundary, surface diffusion on the electrode grains, desorption from electrode grains and diffusion in the electrode pores.

Acknowledgements

This work supported by a grant-in-aid for Scientific Research on Priority Areas of the Ministry of Education, Science and Culture in Japan and Ohkura Kazuchika Foundation. The authors thank Japan New Metals Co. Ltd for supplying the LaB_6 and TiB_2 powders. The a.c. impedance analysis was made using a frequency response analyser at the Center of Advanced Instrumental Analysis, Kyushu University.

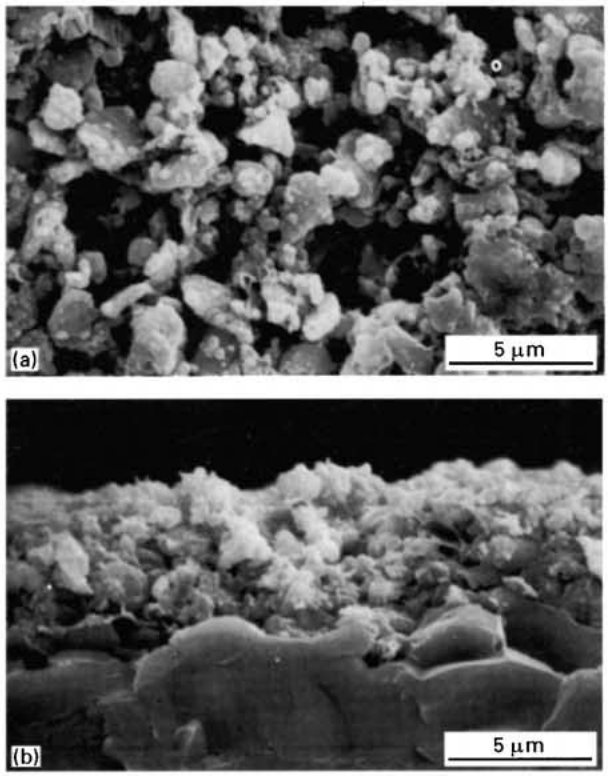

Figure 12 Scanning electron micrographs of TiB_2 film on α-alumina substrate (fired at 900 °C for 1 h in an Ar–H_2 atmosphere).

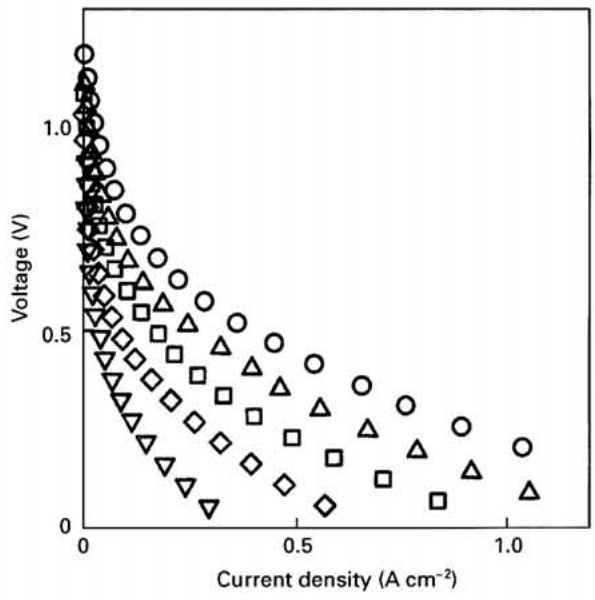

Figure 13 Voltage–current profiles of AMTEC with a TiB_2 electrode: (○) 800 °C, (△) 750 °C, (□) 700 °C, (◇) 650 °C, (▽) 600 °C.

TABLE II Exchange current density and activation energy of LaB_6, TiB_2 and Mo electrodes

Electrode	Particle size (μm)	Thickness (μm)	Exchange current density (mA cm^{-2})					Activation energy (kJ mol^{-1})
			600 °C	650 °C	700 °C	750 °C	800 °C	
LaB_6	0.2	6	0.56	1.00	0.79	1.00	1.2	16
	0.6	2	0.003	0.010	0.017	0.040	0.10	30
		5	0.13	0.32	1.58	3.16	5.0	34
		12	0.40	0.56	1.12	2.51	–	26
	4.5	7	0.50	1.26	4.47	6.31	15.8	30
TiB_2	1–2	5	2.29	2.34	3.63	6.71	11.0	36
Mo	0.05	3–5	–	–	2.44	4.65	8.67	107

References

1. N. WEBER, *Energy Conv.* **14** (1974) 1.
2. T. COLE, *Science* **221** (1983) 915.
3. J. L. LASECKI, R. F. NOVAK, J. R. McBRIDE, J. T. BROCKWAY and T. K. HUNT, in "Proceedings of the 22nd Intersociety Energy Conversion Engineering Conference" (1987) p. 1408.
4. C. P. BANKSTON, T. COLE, R. JONES and R. EWELL, *J. Energy* **7** (1983) 442.
5. C. P. BANKSTON, R. M. WILLIAMS, B. JEFFRIES-NAKAMURA and T. COLE, in "Proceedings of the 22nd Intersociety Energy Conversion Engineering Conference" (1987) p. 1423.
6. T. MASUDA, A. NEGISHI and K. TANAKA, *DENKI KAGAKU* **55** (1987) 197.
7. K. TANAKA, A. NEGISHI, K. NOZAKI and T. MASUDA, *Trans. Jpn Soc. Mech. Eng.* **57** (1991) 239.
8. R. M. WILLIAMS, G. NAGASBRAMANIAN, S. K. KHANNA, C. P. BANKSTON, A. P. THAKOOR and T. COLE, *J. Electrochem. Soc.* **133** (1986) 1587.
9. J. R. McBRIDE, R. F. NOVAK, D. J. SCHMATZ, W. B. COPPLE, J. T. BROCKWAY, N. ARNON and G. A. GRAB, in "Proceedings of the 24th Intersociety Energy Conversion Engineering Conference" (1989) p. 683.
10. O. ASAKAMI, K. TSUCHIDA, H. TOGAWA and A. KATO, *J. Mater. Sci. Lett.* **8** (1989) 1141.
11. T. HASHIMOTO, K. SHIBATA, K. TSUCHIDA and A. KATO, *ibid.* **11** (1992) 745.
12. O. ASAKAMI, K. SHIBATA, T. HASHIMOTO, H. NAKATA, K. TSUCHIDA and A. KATO, in "Proceedings of the 26th Intersociety Energy Conversion Engineering Conference" (Am. Nuclear Soc., Lagrange Park, Illinois, 1991) Vol. 5, p. 469.
13. O. ASAKAMI, K. TSUCHIDA and A. KATO, *J. Mater. Sci. Lett.* **9** (1990) 892.
14. A. KATO, K. TSUCHIDA, T. HASHIMOTO, H. NAKATA and T. NAGATA, in "Proceedings of the 27th Intersociety Energy Conversion Engineering Conference" (SAE Intl. Warrendale, PA, 1992) p. 3.1.
15. H. NAKATA, T. NAGATA, K. TSUCHIDA and A. KATO, *J. Appl. Electrochem. Soc.* **23** (1993) 1251.
16. A. KATO, H. NAKATA and K. TSUCHIDA, in "Proceedings of the 28th Intersociety Energy Conversion Engineering Conference" (Am. Chem. Soc., Washington D.C, 1993) p. 1.809.
17. Q. FANG and R. KNODLER, *J. Mater. Sci.* **27** (1992) 6725.
18. A. KATO, K. TSUCHIDA, T. NAGATA and H. NAKATA, in "Proceedings of the 12th International Conference on Thermoelectrics" (1993) p. 532.
19. H. SUTOH, "Electrode and electrode material" (IPC, Tokyo, 1989) p. 400.
20. R. M. WILLIAMS, M. E. LOVELAND, B. JEFFRIES-NAKAMURA, M. L. UNDERWOOD, C. P. BANKSTON, H. LEDUC and J. T. KUMMER, *J. Electrochem. Soc.* **137** (1990) 1709.
21. R. M. WILLIAMS, B. JEFFRIES-NAKAMURA, M. A. RYAN, M. L. UNDERWOOD, D. O'CONNOR and S. KIKKERT, in "Proceedings of the 27th Intersociety Energy Conversion Engineering Conference" edited by K. Matsuura, (Inst. Electrical Engineer, Japan, 1992) p. 3.19.

Received 25 July 1996
and accepted 22 August 1997